

EVIDENCE FOR EXTENDED, OBSCURED STARBURSTS IN SUBMM GALAXIES

S. C. CHAPMAN,¹ IAN SMAIL,² R. WINDHORST,³ T. MUXLOW⁴ & R. J. IVISON⁵

Received 2004 January 7; accepted 2004 June 29

ABSTRACT

We compare high-resolution optical and radio imaging of 12 luminous submillimeter (submm) galaxies at a median $z = 2.2 \pm 0.2$ observed with *Hubble Space Telescope* (*HST*) and the MERLIN and VLA radio interferometers at comparable spatial resolution, $\sim 0.3''$ (~ 2 kpc). The radio emission is used as a tracer of the likely far-infrared morphology of these dusty, luminous galaxies. In $\sim 30\%$ of the sample the radio emission appears unresolved at this spatial scale, suggesting that the power source is compact and may either be an obscured AGN or a compact nuclear starburst. However, in the majority of the galaxies, $\sim 70\%$ (8/12), we find that the radio emission is resolved by MERLIN/VLA on scales of $\sim 1''$ (~ 10 kpc). For these galaxies we also find that the radio morphologies are often broadly similar to their restframe UV emission traced by our *HST* imaging. To assess whether the radio emission may be extended on even larger scales, $\gg 1''$, resolved out by the MERLIN+VLA synthesized images, we compare VLA B-array ($5''$ beam) to VLA A-array ($1.5''$ beam) fluxes for a sample of 50 μ Jy radio sources, including 5 submm galaxies. The submm galaxies have comparable fluxes at these resolutions and we conclude that the typical radio emitting region in these galaxies are unlikely to be much larger than $\sim 1''$ (~ 10 kpc). We discuss the probable mechanisms for the extended emission in these galaxies and conclude that their luminous radio and submm emission arises from a large, spatially-extended starburst. The median star formation rates for these galaxies are $\sim 1700 M_{\odot} \text{ yr}^{-1}$ ($M > 0.1 M_{\odot}$) occurring within regions with typical sizes of $\sim 40 \text{ kpc}^2$, giving a star formation density of $45 M_{\odot} \text{ yr}^{-1} \text{ kpc}^{-2}$. Such vigorous and extended starburst appear to be uniquely associated with the submm population. A more detailed comparison of the distribution of UV and radio emission in these systems shows that the broad similarities on large scales are not carried through to smaller scales, where there is rarely a one-to-one correspondance between the structures seen in the two wavebands. We interpret these differences as resulting from highly structured internal obscuration within the submm galaxies, suggesting that their vigorous activity is producing wind-blown channels through their obscuring dust clouds. If correct this underlines the difficulty of using UV morphologies to understand structural properties of this population and also may explain the surprising frequency of Ly α emission in the spectra of these very dusty galaxies.

Subject headings: cosmology: observations — galaxies: evolution — galaxies: formation — galaxies: starburst

1. INTRODUCTION

Since their discovery, luminous submm galaxies (SMGs) have been proposed as candidates for the progenitors of the most massive spheroids in the local Universe (Smail, Ivison & Blain 1997; Hughes et al. 1998; Lilly et al. 1999; Blain et al. 2002). The recent measurement of the redshift distribution, space densities and clustering of this population provides strong support for this proposed relationship (Chapman et al. 2003a, 2004; Blain et al. 2004). These galaxies have large bolometric luminosities, $\sim 10^{12}$ – $10^{13} L_{\odot}$, characteristic of ultraluminous infrared galaxies (ULIRGs, Sanders & Mirabel 1996). If their intense restframe far-infrared (far-IR) emission arise from dust-obscured star formation, then the estimated rates are $\gtrsim 10^3 M_{\odot} \text{ yr}^{-1}$, sufficient to form the stellar population of a massive elliptical galaxy in only a few dynamical times, given a sufficient gas reservoir.

Alternatively, a substantial fraction of the submm emission in these galaxies could arise from an obscured AGN

(e.g. Almaini et al. 1999). It has proved difficult to distinguish whether AGN or starburst activity powers the dust heating and associated far-IR radiation in these luminous submm galaxies (Frayser et al. 1998; Alexander et al. 2003; Chapman et al. 2003a). Optical and near-infrared spectroscopy or X-ray observations have frequently been used to search for the signatures of AGN, in both local ULIRGs and those at high-redshifts (Sanders & Mirabel 1996; Fabian et al. 2000; Ivison et al. 2000; Barger et al. 2001; Frayer et al. 2003; Chapman et al. 2003a; Alexander et al. 2003, 2004; Swinbank et al. 2004). However, merely identifying the presence of an AGN within a ULIRG does not immediately mean that it must be the dominant source of far-IR radiation. Energetic arguments must be used to estimate what fraction of a ULIRG's luminosity arises from the AGN.

A much simpler test is available if the far-IR emission is resolved – the geometry of the emission from an AGN means it is not a natural source to heat dust over an ex-

¹California Institute of Technology, MS 320-47, Pasadena, CA, 91125

²Institute for Computational Cosmology, University of Durham, South Road, Durham DH1 3LE, UK

³Arizona State University, Dept. of Physics and Astronomy, Tempe, AZ, 85287-1504

⁴University of Manchester, MERLIN/VLBI National Facility, Jodrell Bank Observatory, Cheshire, SK11 9DL, UK

⁵Astronomy Technology Centre, Royal Observatory, Blackford Hill, Edinburgh EH9 3HJ, UK

tended region – hence any extended far-IR emission is very likely to arise from star formation. Unfortunately, the coarse resolution of most far-IR and submm instruments, e.g. $\sim 15''$ FWHM at $850\ \mu\text{m}$ with SCUBA on the JCMT, means that the emission is rarely resolved except in the most local galaxies (Le Floch et al. 2002). There have been recent claims for the detection of submm emission on $\sim 100\ \text{kpc}$ scales around some powerful high-redshift AGN (Ivison et al. 2000; Stevens et al. 2003, 2004), however, these are rare and extreme objects whose characteristics may have little bearing on those of typical submm galaxies. To disentangle the mechanisms responsible for the far-IR emission in the population of submm galaxies at $z \sim 2\text{--}3$ (Chapman et al. 2003a), will likely require sub-arcsecond resolution to map emission on kpc scales – well beyond the capabilities of current far-IR/submm facilities.

One way to circumvent the limited spatial resolution of far-IR/submm instruments is by exploiting the tight far-IR–radio correlation observed for infrared galaxies (e.g. Helou et al. 1985; Condon 1992) and the high angular resolution capabilities of long-baseline radio interferometers, such as the Multi-Element Microwave Linked Interferometer (MERLIN) or the Very Large Array (VLA), to infer the sub-arcsecond distribution of far-IR emission within submm galaxies. One caveat of this approach is that the far-IR–radio correlation has only been demonstrated locally on relatively large scales, $\sim 50\ \text{kpc}$ (Yun, Reddy & Condon 2001), and it the precise correlation may break down on the smallest scales (M. Yun, in preparation). Nevertheless, if a significant extended component of the continuum radio emission from the submm population is seen then this would provide strong support for the far-IR emission being similarly extended.

The deepest 1.4-GHz observations from the VLA can detect the synchrotron emitting disks and nuclear starbursts (formed from the coalescence of radio supernovae and their remnants) of a ULIRG such as Arp 220 out to redshifts of $z = 3\text{--}4$. Indeed, a large fraction of the bright submm population at high redshifts are detected as μJy radio sources (Smail et al. 2000; Barger, Cowie & Richards 2000; Chapman et al. 2001; Ivison et al. 2002), as expected given their submm luminosities and the local far-IR–radio correlation (Chapman et al. 2004). The highest spatial resolution available from the VLA at 1.4 GHz is $1.5''$, but by combining deep 1.4-GHz observations from MERLIN and the VLA it is possible to produce datasets which combine both high sensitivity and high spatial resolution, $\sim 0.3''$ scales, sufficient to map μJy radio sources and test the extent of the far-IR activity in these galaxies.

These sub-arcsecond radio maps, which indirectly trace the far-IR morphologies, of the SMG population can also be compared and contrasted with the restframe UV structures visible in *HST* imaging on similar scales. Such comparisons may help to constrain the extent of obscuration in SMGs relative to other samples of high-redshift sources selected in the restframe UV (e.g. Adelberger & Steidel 2000).

In this paper, we present sensitive MERLIN/VLA radio

and *HST* restframe UV observations of SMGs at comparable, sub-arcsecond resolution. We discuss the sample and observations in §2, describe our main results in §3 and discuss our conclusions in §4. We assume a Λ -CDM cosmology with $\Omega_0 = 0.3$, $\Omega_\Lambda = 0.7$ and $H_0 = 65\ \text{km s}^{-1}\ \text{Mpc}^{-1}$, so that 1 arcsec corresponds to $8.4\ \text{kpc}$ physical size at $z = 2.2$.

2. SAMPLE AND OBSERVATIONS

Our primary observational dataset is the combined MERLIN⁶ and VLA radio map of a $10' \times 10'$ region centered on the Hubble Deep Field (HDF) region, which has sufficient sensitivity and resolution to attempt a radio morphological analysis of the submm galaxies in this area.

The SMG sample in this region comes from the parent catalog of submm-detected, optically-faint μJy radio galaxies used in the spectroscopic survey of Chapman et al. (2003a, 2004). We identify 14 submm-detected galaxies lying within a $7.5'$ -diameter field centered on 12 36 48.0 +62 15 40 (J2000) which have $850\ \mu\text{m}$ fluxes brighter than $4\ \text{mJy}$ and are detected at 1.4 GHz in the VLA A-array observations of this region with a flux of $> 40\ \mu\text{Jy}$. This radio flux limit should ensure a useful constraint on the source morphology from the MERLIN observations.

2.1. MERLIN Observations

The deep MERLIN observation of the HDF region (Muxlow et al. 1999; Muxlow et al. 2004) comprise ~ 430 hrs integration at 1.4 GHz of a $10' \times 10'$ field centered on the HDF and including the Hubble Flanking Fields (HFF). These data were acquired in February 1996 and April 1997. The MERLIN data were supplemented with 42 hrs of 1.4-GHz VLA⁷ A-array observations (Richards 2000), and combined and deconvolved in the sky-plane due to computational limitations. We use a map with a restored $0.3''$ beam which has an rms noise level of $3.3\ \mu\text{Jy beam}^{-1}$. To register the radio and optical data, radio sources associated with compact galaxies have been used to align the radio map with panoramic ground-based imaging (see below). For the HDF, this matching involves 128 $I < 24$ optical sources with radio counterparts and yields an rms of $0.3''$ (Capak et al. 2004).

2.2. HST imaging

We next search the *HST*⁸ database for deep imaging observations of SMGs that lie within MERLIN field. As our primary goal is a comparison of the coarse morphologies of the sources in the radio and optical wavebands, the choice of camera used for the *HST* observations is less critical than it would be for a detailed morphological analysis of SMGs (Chapman et al. 2003b). Hence, we search for any observations of SMGs within the HDF MERLIN field using the STIS and ACS cameras.

Due to the intensive study of this field we identify *HST* imaging of 13 SMGs from our sample which lie in the MERLIN field and list these in Table 1. Four of these galaxies come from the *HST* targeted survey of 13 SMGs

⁶MERLIN, a UK National Facility operated by the University of Manchester at Jodrell Bank Observatory on behalf of PPARC

⁷The National Radio Astronomy Observatory is a facility of the National Science Foundation operated under cooperative agreement by Associated Universities, Inc.

⁸The optical data is based around observations with the NASA/ESA *Hubble Space Telescope*, obtained at the Space Telescope Science Institute, which is operated by the Association of Universities for Research in Astronomy, Inc., under NASA contract NAS5-26555.

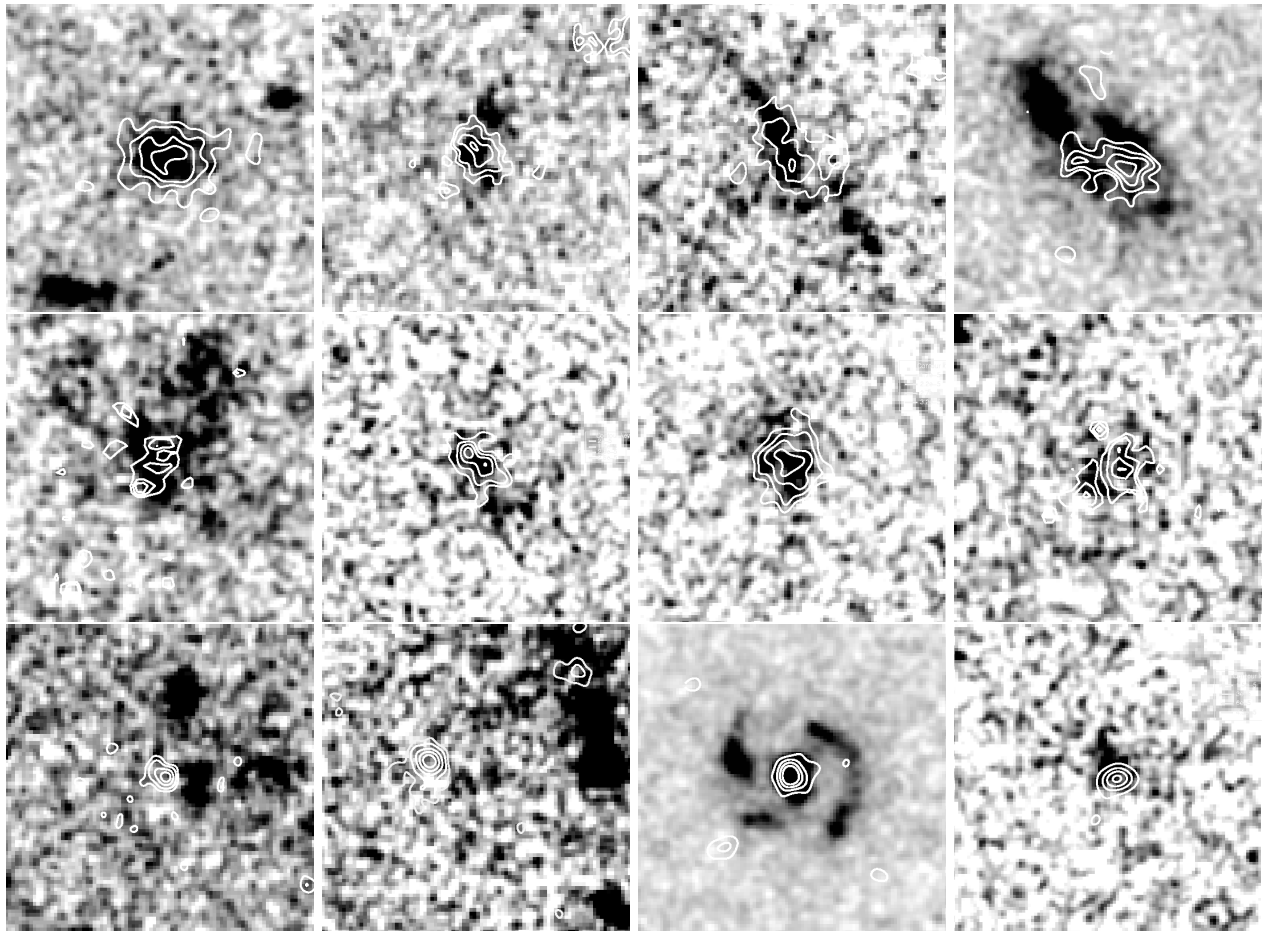


FIG. 1.— Comparison of MERLIN/VLA radio data (0.2–0.3'' synthesized beamsize, shown as contours) for 12 of our SMGs with the *HST* STIS CLEAR50CCD and ACS $b_{435}+i_{775}$ imaging (as noted in Table 1). The *HST* images have been smoothed with a Gaussian of FWHM 0.2'' to match the effective resolution of the radio map. The first two rows show sources where the radio is clearly extended along a portion of the rest-UV imaging, whereas the final four panels on the bottom row reveals point sources in the radio, likely associated with a single UV component. Radio contour levels begin at 3σ and increase in linear steps scaled to the peak of the radio emission. Each panel is 3'' on a side and they are ordered from top-left as in the same sense as Table 1.

observed with STIS by Chapman et al. (2003b), see Table 1. In addition to these, a further 9 SMGs serendipitously fall in the HDF/HFF region which is covered by ACS imaging from the GOODS project (Giavalisco et al. 2004).

However, in one of these 13 sources (SMM J123651.76 +621221.3), the SMG is not uniquely identified, and may lie behind a foreground elliptical galaxy (Dunlop et al. 2004), and an accurate comparison of the morphology using the MERLIN/VLA radio and *HST* in the optical is impossible. We exclude this object from further comparison.

The Cycle 10 STIS imaging of galaxies in our sample uses the open filter, CLEAR50CCD (central wavelength 5733Å), and have durations of two or three orbits (5.0–7.5 ks). The reduction and analysis of these images is described in Chapman et al. (2003b). The resolution of these images is 0.06'' FWHM and they have a typical point-source sensitivity limit of 27.4 mag. (AB).

The ACS observations of the SMGs lying within the GOODS-N field were obtained from the STScI v1.0 release (August, 2003), in the i_{775} and b_{435} bands. The reduction of these data is described by Giavalisco et al. (2004) and the typical point-source sensitivity is 28 mag. (AB) and

resolution of 0.07''.

We register the *HST* images to the radio coordinate frame by aligning them with the deep Suprimecam images from Capak et al. (2004) which are tied to the radio frame. To achieve this we first smooth the *HST* images to the ground-based seeing, then match all $> 5\text{-}\sigma$ sources (except the SMG), and transform the coordinate grids using the IRAF task, GEOTRAN.

The morphological characteristics of this sample have been classified by eye from the *HST* imaging in Fig. 1 and are presented in Table 1. These rough morphological classes are subject to uncertain structured dust extinction (Smail et al. 1999), and may not represent the true physical morphology of the system.

2.3. Archival observations

Optical photometry for our SMG sample in the B and R -bands (Table 1) was measured from the Subaru Suprimecam imaging published by Capak et al. (2004). We use a 3'' diameter aperture centered on the radio source and the limiting magnitudes are $B < 26.9$ and $R < 26.6$ (5σ).

11 of these 12 SMGs in our sample have secure spectroscopic redshifts from the Keck survey of Chapman et al. (2004 – Table 1). These enable us to measure physical

sizes and luminosities for these galaxies and also calculate K-corrections between galaxies in the sample to directly compare their restframe properties. *UgRIK* photometry exists for the remaining source (SMM J123646.1+621449), allowing us to estimate a photometric redshift. Using the HYPER-Z software (Bolzonella et al. 2000), we derive a photometric redshift of $z = 1.7 \pm 0.2$. The median redshift of the sample is $\langle z \rangle = 2.2 \pm 0.2$, representative of that measured for a larger spectroscopic samples of submm galaxies Chapman et al. (2003a, 2004).

3. ANALYSIS AND RESULTS

Using the registered radio and *HST* optical imaging we show in Fig. 1 the 1.4-GHz MERLIN/VLA contours overlaid on the *HST* images for the 12 SMGs in the joint sample. We note that at the median redshift of our sample, the *HST* imaging corresponds to restframe wavelengths of 1700–1800Å. The median diameter of the radio emission from the 12 galaxies is $0.83 \pm 0.14''$ or 7.0 ± 1.1 kpc (measured above the $3\text{-}\sigma$ contour, Fig. 1), showing that the typical source in our sample is well-resolved at the resolution of our MERLIN/VLA map. The radio morphologies for these submm galaxies split into two broad classes: those dominated by an unresolved component, often centered on a sub-component of the *HST*-optical emission (4/12 or 33%), and extended structures on scales $\sim 0.5\text{--}1''$ (8/12 or 67%). Remarkably, the extended radio morphology in these latter sources often appears to trace the same UV-bright, large-scale structures seen in the *HST* optical images (Fig. 1).

With sensitive, high-resolution imagery in the radio and optical, we can compare the radio emission (as a tracer of the dust emission) to restframe-UV emission on kpc-scales within the systems. In Fig. 2 we show the radio and restframe UV surface brightness profiles along the major axes of three representative resolved sources. In some cases the UV emission shows broad similarities to the radio emission. However, Fig. 2 demonstrates that the UV/radio flux ratios can vary significantly over the extent of the galaxy, and the SFRs derived from the respective wavelengths will differ accordingly. For example, in SMM J123621.3+621708 the extended restframe UV emission does not trace the more compact radio emission, with the peak of the radio emission actually coinciding with a clear deficit in the UV emission. Such anti-correlations in the radio and UV are similar to those seen in many local ULIRGs (Chamandarlis et al. 2002).

To test whether there is any evidence for a correlation between internal reddening and the distribution of obscured star formation traced by the radio emission, we construct $(b_{435} - i_{775})$ color maps of the 12 SMGs using the ACS imaging of the GOODS-N region. Only SMM J123712.0+621325 and SMM J123707.2+621408 show redder internal color structure which corresponds to the radio morphology. In all other cases, the radio emission does not correspond to any regions with unusually red colors in the *HST* $(b_{435} - i_{775})$ maps. SMM J123707.2+621408 and SMM J123712.0+621325 actually show bluer colors in the vicinity of the peaks in the radio emission. This suggests that the UV emission may not always probe the true site of far-IR emission; and indeed the UV-inferred bolometric luminosities in SMGs on average underpredict the true

luminosities by factors $\gg 10$ (Chapman et al. 2004).

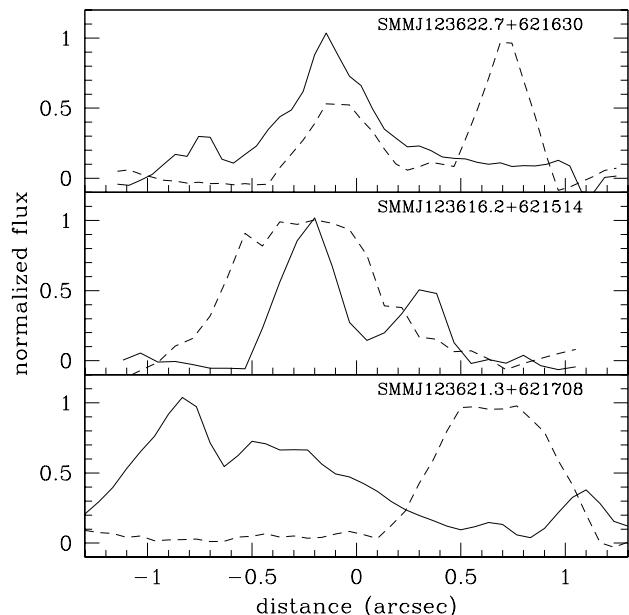


FIG. 2.— The surface brightness profiles in the radio and optical wavebands along the major axes of the radio emission in three of the resolved SMGs. The dashed line shows the radio emission from the MERLIN/VLA map and the solid line shows the equivalent distribution of the restframe UV emission from the *HST* imaging. In both cases the surface brightness is averaged over a $0.3''$ window orthogonal to the major axis. The top axis gives the angular size at the mean redshift of these three galaxies, the variation in their redshifts produces less than a 5% change in angular scale between sources.

A more quantitative test of the degree of obscuration within these galaxies is gleaned through comparing the variation in the total radio/UV flux ratio measurements of each galaxy with that derived locally for the regions of intense far-IR emission pinpointed by the MERLIN/VLA morphology. The monochromatic rest-frame 2000Å luminosities (L_{UV}) of our SMGs are estimated from linear interpolation between the *B*- and *R*-band magnitudes (Table 1).

We estimate L_{FIR} using the measured radio flux (Table 1), K-corrected using synchrotron slope of $\alpha = -0.75$ ($S_\nu \propto \nu^\alpha$) to restframe 1.4 GHz at the observed redshift, and then transformed to the far-IR using the local far-IR–radio correlation from Helou et al. (1985). We take this route to estimate the far-IR emission on arcsecond-scales as our submm data lack both the spatial resolution and full spectral information needed to estimate L_{FIR} more directly. We note that Garrett (2002) and Kovacs et al. (2004) have shown that the far-IR–radio relation does not seem to be change substantially out to $z \sim 1\text{--}2.5$, and so the approach we have adopted should be reliable. In this manner we predict a median total, far-IR luminosity of $(3.5 \pm 1.0) \times 10^{12} L_\odot$ for the 12 SMGs, equivalent to star formation rates of $\sim 1700 M_\odot \text{yr}^{-1}$ for stars more massive than $0.1 M_\odot$ based on a Salpeter IMF.

To investigate the variation of far-IR/UV ratios within the SMGs we first calculate the ratios for the total emission from the galaxies. We then measure the same ratio in a region encompassing the peak of the radio emission using a fixed circular aperture enclosing all radio emission above the 3σ contour shown in Fig. 1. We compare the total and locally derived $L_{\text{FIR}}/L_{\text{UV}}$ ratios for the 12 sources in Fig. 3. We see that when the regions pinpointed as the sites of strong activity by the MERLIN/VLA radio morphology are considered, the obscuration levels increase by factors of 2–8 over the ratios derived for the whole galaxy. Even measured over the entire extent of the systems, the obscurations we derive are considerably higher than those seen in high redshift, restframe UV-selected populations which are typically $L_{\text{FIR}}/L_{\text{UV}} \sim 0.1\text{--}100$ (e.g. the Lyman-break galaxies, Adelberger & Steidel 2000; or the BX/BM galaxies, Steidel et al. 2004).

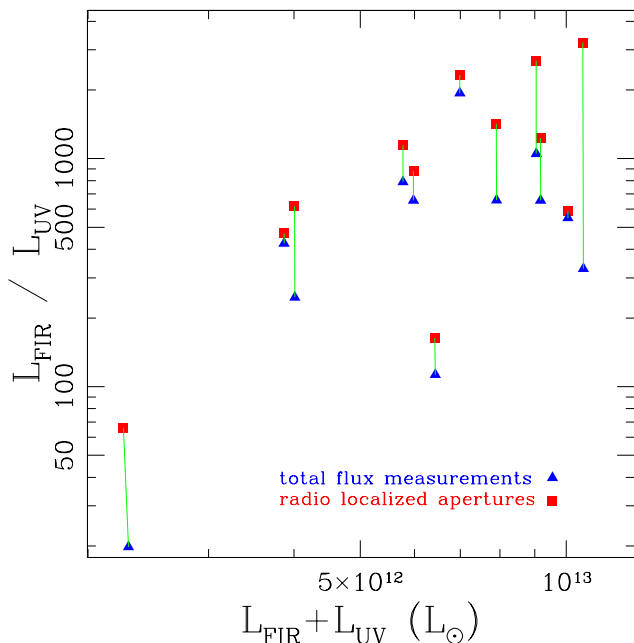


FIG. 3.— The ratio of far-IR luminosity to restframe UV luminosity (2000Å monochromatic luminosity) plotted against total luminosity (far-IR + UV) for the 12 SMGs which are detected in the MERLIN+VLA map. We show data points corresponding to the ratio derived from total flux measurements of each source using MERLIN+VLA for radio and *HST* for the restframe UV, and based on small aperture measurements in the UV and radio based on the positions of the peak of the radio emission in the MERLIN+VLA map (Muxlow et al. 2004).

3.1. Searching for very extended radio emission

Having discovered that the radio emission in over half the SMGs in our sample is extended on $1''$ scales we now wish to test whether this emission extends to even larger scales, $\geq 5''$ or ~ 50 kpc. We can constrain the fraction of radio flux arising on $\geq 1.5''$ scales by a simple comparison of the 1.4-GHz fluxes of SMGs in maps from the VLA in its B-array ($5''$ synthesized beam) and A-array ($1.5''$ beam) configurations. The higher resolution A-array observations

may resolve out a portion of the total emitted flux density of any source which has significant extended structure on scales larger than the $1.5''$ VLA A-array beam. As no B-array coverage is available for the HDF-N we have assembled VLA B-array and A-array fluxes for a sample of $50 \mu\text{Jy}$ radio sources, including 5 submm galaxies, from the our SSA22 survey field (see Chapman et al. 2004).

We calculate the median and bootstrap errors on the flux ratios for the radio sources from the data taken at the two resolutions. We start by confirming that sources show either similar or higher fluxes in the B-array map compared to the A-array data, as expected considering the median radio angular sizes of μJy sources (Windhorst et al. 1993) We find median ratios of $\langle S_B/S_A \rangle = 1.45 \pm 0.27$ and that for 30% of the sample agree within $2\text{-}\sigma$, suggesting there is no calibration offset between the fluxes from the two maps. For the five submm-detected sources we obtain a median flux ratio of $\langle S_B/S_A \rangle = 1.22 \pm 0.12$, compared to $\langle S_B/S_A \rangle = 1.22 \pm 0.11$ for an *R*-band matched sample of 8 radio sources undetected or unobserved in the submm waveband. This suggests that the submm-luminous section of the μJy radio populations is no more extended than the general population, after we have removed low redshift galaxies (with bright apparent magnitudes). Moreover, we see that there is only weak evidence that the radio emission in the SMGs is extended on $\gg 10$ kpc scales.

4. DISCUSSION & CONCLUSIONS

The far-IR emission from local ULIRGs generally arises from the nuclear regions of the systems, while the UV light is more extended, although it contributes a negligible fraction of the bolometric emission (Goldader et al. 2002; Surace & Sanders 2000). We have been able to trace the distribution of these two components in similarly luminous galaxies at high redshifts through the combination of sub-arcsecond imagery in the radio and restframe UV from our MERLIN/VLA and *HST* observations. These maps allowed us to investigate the relative distribution of obscured and unobscured star formation on kpc-scales within luminous submm galaxies at $z \sim 2.2$, when the Universe was only a fifth of its current age.

As expected the UV morphologies of this sample are similar to the (overlapping) sample of submm galaxies imaged with *HST*/STIS and analysed by Chapman et al. (2003b), as well as the ACS imaging in Smail et al. (2004). The sample exhibits irregular and frequently highly complex morphologies in their restframe $\sim 2000\text{\AA}$ emission compared to optically-selected galaxies at similar redshifts, and have scale lengths far in excess of comparably luminous local galaxies.

Turning to the radio morphologies, we find that in $\sim 70\%$ (8/12) the MERLIN/VLA radio exhibits resolved radio emission on $\sim 0.5\text{--}1''$ scales (~ 10 kpc) which mirrors the general form of the restframe UV morphology seen by *HST*. We interpret this as strong support for the radio emission tracing spatially-extended, massive star formation within these galaxies. This situation is very unlike local ULIRGs, where the high surface brightness far-IR/radio emission is restricted to a compact nuclear region with an extent of less than ~ 1 kpc (Charmandaris et al. 2002). A more detailed analysis of the distribution of UV and radio emission within these galaxies (Fig. 2 & 3)

shows that the correspondence is rarely one-to-one, with variations of the UV/radio flux ratio of factors of a few on kpc-scales within galaxies. It is likely that comparisons using even higher resolution data would show even stronger variations, as are seen in local ULIRGs (e.g. Bushouse et al. 2002), but which are diluted at the current resolution. Similarly, there is only weak evidence for correlations between the restframe UV colors and the positions of the radio emitting regions within these galaxies. Here, longer wavelength near-IR observations with *HST*/NICMOS, or from the ground, may reveal variations in the UV spectral slope that would show a better correlation of reddening with radio intensity (Smail et al. 2004).

In the remaining $\sim 30\%$ (4/12) of SMGs, the radio emission is much more compact and is essentially unresolved – suggesting it arises in a region with a scale size of order ~ 1 kpc or less (Fig. 1). In two of these cases, the compact radio emission is centered on a bright UV source (in one case clearly the nucleus of a face-on spiral galaxy, which is a strong X-ray source and is also the only one of the sources in our sample which shows AGN signatures in its UV spectrum), while in the other two systems the compact radio component is spatially offset by several kpc from the UV source. These configurations reflect either compact, nuclear starbursts and/or a dominant contribution from an AGN to the radio emission. In half of these cases the AGN/nuclear starburst is also strongly obscured at restframe wavelengths of $\sim 2000\text{\AA}$.

Stevens et al. (2003, 2004) have recently presented evidence for submm emission resolved on ~ 100 kpc scales (including apparent filaments) in the rare and extreme environments around powerful radio galaxies and absorbed QSOs at $z \sim 2-4$. Our results demonstrate that in many cases ($\sim 70\%$) the far-IR emission (as seen in our MERLIN/VLA radio maps) of the general SMG population is extended on scales ~ 10 kpc. However, the interferometric measurements are not suited to measuring larger scale, diffuse emission. Our VLA B-array versus A-array comparison (§3.2), however, suggests that the typical field SMG does not have submm emission (as traced by the radio) extending on scales much larger than $\geq 1''$ (≥ 10 kpc).

Our high resolution radio and optical imaging allows us to address the relative obscuration of the galaxies. Adelberger & Steidel (2000) have suggested that high-luminosity galaxies at high redshift have much stonger obscuration than lower-luminosity galaxies, as measured by the ratio of far-IR to restframe-UV luminosity. This is certainly true on large-scales in the submm galaxies. On smaller scales within the SMGs, we have seen that the obscuration is roughly $\sim 2\times$ higher over the region of intense radio (and by implication far-IR) emission, compared to the average over the whole galaxy. This suggests that there is highly structured reddening within the submm galaxies, such anisotropic obscuration would be a natural consequence of channels being blown through the dust around the star-formation regions by vigorous winds.

It is worth considering that few star-burst galaxies with $L_{\text{FIR}} \sim 4 \times 10^{12} L_{\odot}$ exist locally; most galaxies in our neighborhood with these luminosities have strong and obvious AGN components. However, at $z \sim 2.2$, the median

redshift of the radio-selected SMGs, the most active galaxies were evidently forming stars at rates of $\sim 1700 M_{\odot} \text{yr}^{-1}$ in regions extending over $\sim 40 \text{kpc}^2$. The large physical extent of this activity contrasts markedly with the compact, nuclear starbursts typical of local redshift ULIRGs. This suggests that the some of the observational properties of the star formation activity in these galaxies (e.g. mix of dust temperatures, ease of superwind generation, etc.) may differ markedly from that seen in local “analogs”. However, we also note that the star formation surface density inferred from our radio observations is $\sim 45 M_{\odot} \text{yr}^{-1} \text{kpc}^{-2}$, comparable to the upper-limit estimated for such activity in local starburst galaxies by Meurer et al. (1997). This argues that the small-scale physical mechanisms which limit the star formation process within these galaxies are similar to those operating in the most vigorous systems locally.

While evidence for massive amounts of molecular gas in submm galaxies has now been established (Frayser et al. 1998; Neri et al. 2003; Greve et al. in preparation), and X-ray luminosities are consistent with a dominant role for star formation in the energetics of SMGs (Alexander et al. 2004), our discovery of spatially extended radio morphologies is perhaps the strongest piece of evidence that star formation dominates the bolometric output of the majority of the submm galaxy population.

In summary, we have compared the restframe UV and radio morphologies on sub-arcsecond scales of a small sample of highly luminous, dusty galaxies for which precise redshifts are available. This analysis shows that the radio emission, which we adopt as a proxy for the far-IR emission, in these galaxies is resolved in the majority of galaxies – implying that dust heating (and by implication, massive star formation) is occurring on ~ 10 kpc scales within these systems. Currently, this represents our only constraint on the likely submm morphology of these galaxies, and one which will not be further testable until ALMA comes online. The overall structure of the radio emission matches that seen in the restframe UV – although there are strong variations in the relative emission on kpc-scales – which we interpret as resulting from highly structured dust obscuration within the galaxies. This structured obscuration may reflect from anisotropic dispersal of the dust as superwinds driven by the star formation activity blows channels through the intergalactic medium. Such channels would provide the opportunity for $\text{Ly}\alpha$ photons to escape from these otherwise highly-obscured systems, explaining the unexpected strength of this line in their spectra (Chapman et al. 2003a, 2004).

We would like to thank the anonymous referee for helpful comments which improved the clarity of the manuscript. We also thank our collaborator, Andrew Blain, for his work on the Keck SMG redshift survey. Support for proposal #9174 (SCC, RW) was provided by NASA through a grant from the Space Telescope Science Institute, which is operated by the Association of Universities for Research in Astronomy, Inc., under NASA contract NAS5-26555. IRS acknowledges support from the Royal Society and Leverhulme Trust.

TABLE 1
PROPERTIES OF THE SUBMM GALAXIES

^a The radio source extends over 3.3'' predominantly to the west of the galaxy. Some very low surface brightness emission is missed in the MERLIN image which just shows three components. There is extended emission between these sources.

^b Two resolved radio sources trace the two faint UV-detected sources within a 1'' region.

^c Two radio sources are found within the SCUBA error circle, the brighter one listed in the table lacks an optical ID, and the fainter one associated with a linear galaxy 2'' to the east (see Fig. 1).

^d This source was identified in Hughes et al. (1998) as HDF 850.2

^e HST imaging from STIS, otherwise with ACS.

^f Radio morphologies: extended (E) or compact (C).

Source	z	B	R	S_{850} (mJy)	$S_{1.4}$ (μ Jy)	Morphology ^f	
						Radio	Optical
SMM J123606.9+621021	2.509	25.6	25.2	11.6 \pm 3.5	74.4 \pm 4.1	E	Disturbed, merger
SMM J123616.2+621514 ^e	2.578	26.8	25.7	5.8 \pm 1.1	53.9 \pm 8.4	E	3 components
SMM J123622.7+621630 ^e	2.466	25.6	25.4	7.7 \pm 1.3	70.9 \pm 8.7	E	Merging disks
SMM J123629.1+621046 ^a	1.013	26.1	24.6	5.0 \pm 1.3	81.4 \pm 8.7	E	Disturbed
SMM J123655.8+621200 ^d	2.743	25.4	25.3	8.0 \pm 1.8	21.0 \pm 6.2	E	Disturbed, merger
SMM J123707.2+621408	2.484	26.9	26.0	6.3 \pm 1.3	45.3 \pm 7.9	E	Blue & red pair
SMM J123712.0+621325	1.992	26.0	25.8	4.1 \pm 1.3	53.9 \pm 8.1	E	Disturbed with dusty component
SMM J123712.1+621212 ^b	2.914	27.0	25.5	8.0 \pm 1.8	21.0 \pm 4.0	E	Disturbed, double source
SMM J123618.3+621551 ^e	1.865	26.0	25.9	7.3 \pm 1.1	150.5 \pm 11.2	C	Small group
SMM J123621.3+621708 ^{c,e}	1.988	25.1	24.9	7.8 \pm 1.9	148.1 \pm 11.2	C	Linear
SMM J123635.6+621424	2.005	24.2	24.2	5.5 \pm 1.4	87.8 \pm 8.8	C	Disturbed, face-on spiral
SMM J123646.1+621449	1.7	25.8	25.7	10.3 \pm 2.2	124.3 \pm 7.9	C	Disturbed (photo-z)

REFERENCES

- Adelberger K., Steidel C., 2000, ApJ, 544, 218
 Alexander D., Vignali C., Bauer F.E., Brandt W.N., Hornschemeier A.E., Garmire G.P., Schneider D.P. 2002, AJ, 123, 1149
 Alexander D., Smail I., Bauer F., Chapman S., Blain A., Ivison R., 2004, Nature, submitted
 Almaini O., Lawrence A., Boyle B.J., 1999, MNRAS, 305, L59
 Barger A., Cowie L., Richards E., 2000, AJ, 119, 2092
 Barger, A., Cowie L., Mushotzky R., Richards E., 2001, AJ, 121, 662
 Blain A., et al. 2002, Phys. Rep., 369, 111
 Blain A., et al. 2004, ApJ, 611, 725
 Bolzonella, M., Miralles, J.-M., Pello, R., 2000, A&A, 363, 476
 Bushouse, H.A., Borne, K.D., Colina, L., Lucas, R.A., Rowan-Robinson, M., Baker, A.C., Clements, D.L., Lawrence, A., Oliver, S., 2002, ApJS, 138, 1
 Capak P., et al., AJ, 2004, in press
 Chapman, S. C., Richards, E.A., Lewis, G. F., Wilson, G., & Barger, A. J. 2001, ApJ, 551, L9
 Chapman S.C., Blain A., Ivison R., Smail I., 2003a, Nature, 422, 695
 Chapman S. C., Windhorst R., Odewahn S., Yan H., Conselice C., 2003b, ApJ, 599, 92
 Chapman S. C., Blain A., Smail I., Ivison, R., 2005, ApJ, in press
 Charmandaris, V., Stacey, G.J., Gull, G., 2002, ApJ, 571, 282
 Condon J.J. 1992, ARA&A, 30, 575
 Dunlop J., et al. 2004, MNRAS, in press
 Fabian A.C., et al., 2000, MNRAS, 315, L8
 Frayer D., et al., 1998, ApJ, 560, 7
 Frayer D., et al., 2003, AJ, 126, 73
 Garrett M., 2002, A&A, 384, 19
 Giavalisco M., et al. 2004, ApJ, 600, L93
 Goldader J., Meurer G., Heckman T., Seibert M., Sanders D., Calzetti D., Steidel C., 2002, ApJ,
 Helou, G., et al., 1985, ApJ 440, 35
 Hughes D., et al. 1998, Nature, 394, 241
 Ivison R., et al., 2000, MNRAS, 315, 209
 Ivison et al. 2002, MNRAS, 359, 1
 Kovacs A., et al. 2005, in preparation
 Le Floc'h E., Charmandaris V., Laurent O., Mirabel F., Gallais P., et al. 2002, A&A, 391, 417
 Lilly S., Eales S., Webb T., Dunne L., Gear W., Clements D., Yun M., 1999, ApJ, 518, 614
 Muxlow T., et al., 1999, New Astronomy, 43, 623
 Muxlow T., et al., 2004, MNRAS, in preparation
 Neri, R., et al., 2003, ApJ, 597, L113
 Richards E., 2000, ApJ, 533, 611
 Sanders D.B., Mirabel I.F. 1996, ARA&A, 34, 749
 Smail, I., Ivison, R.J., Blain, A.W., 1997, ApJ 490, L5
 Smail, I., Morrison, G., Gray, M.E., Owen, F.N., Ivison, R.J., Kneib, J.-P., Ellis, R.S., 1999, ApJ, 525, 609
 Smail, I., Ivison R.J., Owen F.N., Blain A.W., Kneib J.-P. 2000, ApJ, 528, 612
 Smail, I., et al., 2004, ApJ, in press
 Steidel C., et al., 2004, ApJ, in press
 Stevens J., et al., 2003, Nature, 425, 264
 Stevens J., et al., 2004, ApJ, 604, L17
 Surace J., Sanders D., 2000, AJ, 120, 604
 Swinbank, A.M., et al., 2004, ApJ, in press
 Windhorst R., et al. 1993, ApJ, 405, 498
 Yun M., Reddy N., Condon J. 2001, ApJ, 554, 803